Title: Effects of Ni and TiO_2 additions in as-reflowed and annealed Sn0.7Cu solders on Cu substrates

Author: M.A.A. Mohd Salleh S.D. McDonald K. Nogita

PII: S0924-0136(16)30426-5
DOI: http://dx.doi.org/doi:10.1016/j.jmatprotec.2016.11.031
Reference: PROTEC 15032

To appear in: *Journal of Materials Processing Technology*

Received date: 22-6-2016
Revised date: 26-9-2016
Accepted date: 25-11-2016

Please cite this article as: Mohd Salleh, M.A.A., McDonald, S.D., Nogita, K., Effects of Ni and TiO2 additions in as-reflowed and annealed Sn0.7Cu solders on Cu substrates.Journal of Materials Processing Technology http://dx.doi.org/10.1016/j.jmatprotec.2016.11.031

Effects of Ni and TiO_2 additions in as-reflowed and annealed Sn0.7Cu solders on Cu substrates

M. A. A. Mohd Salleh[a,b*], S. D. McDonald[a], K. Nogita[a]

[a]*Nihon Superior Centre for the Manufacture of Electronic Materials (NS CMEM), School of Mechanical and Mining Engineering, The University of Queensland,4072 St Lucia, Queensland, Australia.*

[b]*Centre of Excellence Geopolymer and Green Technology, School of Materials Engineering, Universiti Malaysia Perlis (UniMAP), Taman Muhibbah 02600, Jejawi, Arau, Perlis, Malaysia.*

*Corresponding author: Room 634, 49 Jocks Rd., St Lucia, Brisbane, QLD 4072, Australia

Email: m.mohdsalleh@uq.edu.au / arifanuar@unimap.edu.my ; Tel: +61 435 946 670

Abstract

The growth of Cu_6Sn_5 and Cu_3Sn_5 interfacial layers after isothermal annealing and the resultant effect on the solder joint strength are studied in TiO_2 and Ni containing Sn0.7Cu solders. These composite solders were fabricated using a powder metallurgy method and reflow soldered on a Cu substrate printed circuit board (PCB) with an organic soldering preservative (OSP) surface finish. With TiO_2 additions, a more planar scalloped Cu_6Sn_5 morphology was observed with reduced interfacial boundary grooves while a fine scallop-shaped interfacial $(Cu,Ni)_6Sn_5$ layer was observed in Ni containing solder joints. The interfacial layer was further suppressed with a combination of Ni and TiO_2 even after annealing which resulted in superior shear strength and fracture energy.

Keywords: Lead-free solder, Reflow soldering, Microstructure, Intermetallic, Interfacial reaction, Shear strength

1.0 Introduction

Intermetallic phases such as Cu_6Sn_5 and Cu_3Sn often form at the solder/substrate interface in many Pb-free solder joints. During thermal ageing, the interfacial intermetallic layer may grow and Kirkendall voids often form at the Cu_6Sn_5/Cu substrate interface. The brittle interfacial intermetallic layer and voids at the solder joint interface can deteriorate the solder joint reliability where cracks may be initiated and propagate. Hence, controlling the thickness of interfacial intermetallics and minimising void formation can improve solder joint reliability.

Ceramic reinforcement of solder matricies with a variety of micrometer or nanometer-size particles such as silicon carbide (SiC), nickel oxide (NiO), alumina (Al_2O_3), zirconia (ZrO_2), titanium oxide (TiO_2) and silicon nitride (Si_3N_4) has been proposed by Mohd Salleh et al. (2013) as a method of suppressing the growth of Cu_6Sn_5 interfacial intermetallic layers during soldering. Chellvarajoo and Abdullah (2016) showed that additions of 2.5 wt% NiO in a Sn3.0Ag0.5Cu solder alloy resulted in a reduction of 60% thickness of the intermetallic layer after a single reflow. However, Shen and Chan (2009) reported that additions of ZrO_2

suppressed the intermetallic layer observed in a Sn9Zn/Cu solder joint after five reflow cycles. During single and multiple reflow cycles, Said et al. (2016) reported that the suppression of the intermetallic layer could be more significant during isothermal annealing.

Various hypotheses exist relating to how the interfacial intermetallic layer is suppressed by additions of particle reinforcements. Chuang et al. (2010) hypothesized that the Al_2O_3 nanoparticles are absorbed in a liquid nanocomposite solder/Cu substrate interface which then suppresses the Cu dissolution in the liquid solder and in return reduces the formation of Cu_6Sn_5 intermetallic compound (IMC) layer. In addition, El-Daly et al. (2013) hypothesized that SiC nanoparticles could act as additional nucleation sites where the rate of solidification of β-Sn will be faster and limit the time for the Ag_3Sn and Cu_6Sn_5 to grow. This mechanism was also reported by Liu et al. (2013) in the reinforcing of Sn-Ag-Cu solder alloys with graphene nanosheets which enhanced the thermodynamic resistance to IMC growth and reduced diffusion.

A growing body of research exists relating to the development of Sn0.7Cu alloys through reinforcement additions. This includes additions of either metallic or non-metallic particles to the solder. Somidin et al. (2013) investigated the effect of additions of aluminum particles to Sn0.7Cu showing both thin Cu_9Al_4 and Cu_6Sn_5 intermetallic layers were formed. Mohd Salleh et al. (2011) and Mohd Salleh et al. (2012) have concluded that additions of Si_3N_4 could enhance the wettability and reduce the Cu_6Sn_5 intermetallic layer thickness and have shown that the shear joint strength could be significantly improved. In addition, Tsao et al. (2012) had investigated the mechanical and thermal properties of TiO_2 reinforced Sn0.7Cu bulk solder. In their report, the melting temperature of the reinforced solder was able to be reduced and an improvement of hardness and tensile strength of the bulk solder was achieved. It has also been reported by Zeng et al. (2014) that Ni additions to Sn0.7Cu solder alloys suppress the Cu_3Sn layer intermetallic layer which typically forms between the Cu_6Sn_5/Cu interface as a result of continuous Cu diffusion from the substrate into the Cu_6Sn_5 layer. Besides the suppression of the intermetallic layer, Mohd Salleh et al. (2016a) revealed that primary Cu_6Sn_5 in the bulk could be significantly refined with Ni additions. In Sn-Ag-Cu solders, additions of Ni were reported by Chuang and Lin (2003) to also effectively suppress the Cu_6Sn_5 layer. Shohji et al. (2005) had also proved that additions of Ni to Sn-Ag-Cu solder were able to suppress the layer after annealing and subsequently improves the solder joint shear strength on Cu substrate after 1000 hours at 100˚C annealing.

This paper investigates the effects of Ni, TiO_2 and combination of both additions in the suppression of the interfacial intermetallic compound after isothermal annealing and their effects on the solder joint mechanical performance by means of high speed shear testing. This includes investigating the solder joint strength, fracture deformation energy and analysis of the failure mode. In addition, we also seek to understand the presence of TiO_2 reinforcement in the solder joints and how it suppresses the interfacial intermetallic layer.

2.0 Experimental

2.1 Sample and solder ball fabrication

Chellvarajoo and Abdullah (2016) reported that most of the methods used to fabricate reinforced solders involve mixing reinforcement particles into a solder paste (a mixture of flux and solder spheres) where due to the buoyancy of the flux and outgassing and density differences, reinforcement particles were observed to be concentrated on the surface of the solder joint after being pushed out during the soldering process. Thus, to reduce the possibility of reinforcement push-out by excessive flux in solder pastes and to obtain a homogenous reinforcement of distribution in the solder matrix, Mohd Salleh et al. (2015a) have previously developed a method of fabricating a preform TiO_2 reinforced solder by a powder metallurgy microwave sintering method. This homogeneous distribution of reinforcement allows the mechanisms of interfacial intermetallic layer suppression to be investigated with more confidence. In preparing the samples, Sn0.7Cu and Sn0.7Cu0.05Ni solder powders of spherical shape (45 µm average particle size) were supplied by Nihon Superior Co. Ltd. for the base matrix materials, along with 99.7% purity TiO_2 anatase powder supplied by Sigma Aldrich Co. (<50 nm average particle size). Table 1 and 2 presents the chemical compositions of the solder powders used as base alloys as obtained using optical emission spectroscopy. Four different solder composition were prepared including Sn0.7Cu, Sn0.7Cu0.05Ni, Sn0.7Cu+TiO_2 and Sn0.7Cu0.05Ni+TiO_2. To fabricate the reinforced solders, 1wt% of TiO_2 particles were incorporated into the base solder matrix using a powder metallurgy route. The TiO_2 reinforcement was homogeneously mixed with the base matrix powder (Sn0.7Cu alloy and Sn0.7Cu0.05Ni) separately in an airtight container using a tubular mixer for 1 hour. The solder mixtures were uniaxially compacted in a 12-mm diameter mold at 120 bar, and the compacted discs were microwave sintered in an inert argon atmosphere. Using a microwave oven with an output power of 1,000W at full power, approximately 3 minutes of microwave sintering time

was taken to achieve the sintering temperature of 185°C (~0.8T_m). For comparison the base materials, Sn0.7Cu alloy and Sn0.7Cu0.05Ni alloys were prepared by compacting the Sn0.7Cu and Sn0.7Cu0.05Ni solder powders respectively and sintered using the same method as the reinforced solders. Sintered samples were then cold rolled to produce thin solder sheets of approximately 23 µm thickness.

In fabricating solder balls, thin solder sheets were punched using a 2.5 mm diameter metal punch to form a thin solder discs. The thin solder discs were then dipped in a rosin mildly activated (RMA) flux and placed on a Pyrex sheet. Using a controlled heating temperature, the solder discs were melted using a reflow oven at 250°C maximum temperature with the aid of N_2 gas flow. Due to the solder melting and the action of surface tension, solder sheets were transformed to solder balls of spherical shape with an approximate diameter of 600 µm. Solder balls were passed through sieves to ensure a uniform size. The fabricated solder balls with small amount of RMA flux were then placed on a Cu substrate printed circuit board (PCB) with an organic soldering preservative (OSP) surface finish and were solder reflowed at 127 s of reflow time at 250 °C maximum temperature with the aid of small amount of flux using a desktop reflow oven with N_2 gas flow. The solder reflow temperature profile used in preparing the solder joints is shown in Figure 1a.

2.2 Isothermal ageing and microstructure analysis

The growth of the interfacial intermetallic compound growth was studied by conducting isothermal annealing experiment at 150°C for 0, 500, 1000, 1500 and 2000 hours. In ensuring temperature uniformity throughout the samples during isothermal ageing, solder joints were isothermally annealed in an oven with a mechanical convection heating system supplied by Thermo Scientific.

Solder joints were then cross-sectioned for microstructure observations. The microstructures of the samples were analysed using a JEOL 6610 SEM/energy dispersive X-ray spectroscopy (EDS) in secondary and backscattered electron imaging mode at an accelerating voltage of 20 kV. For a top-down view of the intermetallic formation, solder joints were etched using solution of 2% 2-nitrophenol, 5% sodium hydroxide and 93% of distilled water. Before detailed SEM imaging and EDS were conducted, samples were thoroughly cleaned and rinsed using acetone in an ultrasonic bath. The interfacial IMC thickness of each sample was measured

using ImageJ software. An average of the interfacial IMC thickness in each image was measured by dividing the total area by the total length.

2.3 High speed shear solder joint evaluation

In evaluating the solder joint strength of samples after isothermal ageing, solder joints were sheared using a Dage 4,000 high speed bond tester with a 60 µm shear height. A 50 N shear load cartridge was used at a 2,000 mm/s shear speed. The high speed shear test sample positioning is as in Figure 1b. Shear strength of the solder joints was determined by means of the maximum shear force of each solder ball shear test conducted while the total shear energy were determined by the total area of shear force and displacement. Shear fracture initiation energy was determined base on the area of shear force and displacement graph from shear initiation until the maximum shear force while the shear fracture propagation energy was determined by the area from maximum shear force until the end of shear displacement. After high speed shear tests were conducted, samples were examined using scanning electron microscopy (SEM) to analyse the fracture surface and failure modes of each of the sheared solder joints. Failure mode distribution was analysed base on four different failure modes classified as ductile (100% area with bulk solder), quasi-ductile (>50% area with bulk solder), quasi-brittle (>50% area with exposed interfacial layer) and brittle (100% area with exposed interfacial layer) as shown in Figure 1a-f respectively.

3.0 Results and Discussion

3.1 Microstructure of annealed solder joints

Microstructure formations particularly on the growth of interfacial intermetallic layers in Sn0.7Cu, Sn0.7Cu+TiO_2, Sn0.7Cu0.05Ni, Sn0.7Cu0.05Ni+TiO_2 solder joints after isothermal annealing were investigated. As in Figure 2a-d, it was observed that in Sn0.7Cu solder joints, a scallop-shape interfacial Cu_6Sn_5 layer had formed with a planar layer of Cu_3Sn. Both Cu_6Sn_5 and Cu_3Sn grew during isothermal annealing and became significantly thicker after 2000 hours of annealing. As in Figure 2d, after 2000 hours the scalloped morphology of the interfacial Cu_6Sn_5 in Sn0.7Cu solder joints had become coarser and flatter compared to the as-reflowed, 500, 1000 and 1500 hours of annealing conditions. In contrast, Figure 2e-f shows the formation and growth of interfacial Cu_6Sn_5 and Cu_3Sn of Sn0.7Cu with TiO_2 additions after isothermal annealing. It was observed that with additions of the reinforcement, a flatter Cu_6Sn_5 layer

formed with a less scallop-shaped morphology compared to the Sn0.7Cu solder joints. However, the interfacial Cu_3Sn layer of the reinforced Sn0.7Cu was slightly thicker compared to the non-reinforced Sn0.7Cu. As reported by Mohd Salleh et al. (2016b), the grooves between the Cu_6Sn_5 scallops play a critical role in the growth of Cu-Sn interfacial layer and during annealing, the grooves serves as diffusion paths of Cu into the solder. It is also reported that during soldering, the TiO_2 particles come into intimate contact with the Cu_6Sn_5 interfacial layer modifying the Cu diffusion and dissolution path into the molten solder and preventing individual Cu_6Sn_5 grains from growing further and reducing the Cu_6Sn_5 channels. One result of less Cu_6Sn_5 groove formation during soldering is that subsequent Cu diffusion from the substrate during thermal annealing will be unbalanced and the growth of the Cu_3Sn layer will be favoured. Besides that, as shown in Figure 2, in both the reinforced and non-reinforced Sn0.7Cu, Kirkendall voids on the Cu_3Sn layer were observed to increase after longer annealing times. Studies made by Yu et al. (2016) reported that Kirkendall voids were introduced by an unbalanced diffusion at the interface and are promoted by higher temperature and annealing times.

Comparing the 0.05wt% Ni additions to Sn0.7Cu, as in Figure 3a-d, the formations of interfacial $(Cu,Ni)_6Sn_5$ layer were rather finer scallop-shape and becomes courser after a longer annealing time. With additions of TiO_2 reinforcement to the Sn0.7Cu0.05Ni as in Figure 3e-h, the morphology of the interfacial layer was similar to the non-reinforced solder joints. However, a thinner interfacial $(Cu,Ni)_6Sn_5$ layer was observed. From cross-sectioned microstructure observations on Sn0.7Cu0.05Ni samples regardless of reinforcement additions, fine primary $(Cu,Ni)_6Sn_5$ were observed near the interfacial layer. From Mohd Salleh et al. (2016a) study, this fine primary $(Cu,Ni)_6Sn_5$ forms in the bulk solder and sinks to the interfacial layer during solidification. In Sn0.7Cu, primary Cu_6Sn_5 particles were larger and the majority were in the bulk solder. Figure 4a-c and 4d-f shows the interfacial intermetallic layer and primary intermetallic morphology after 2000 hours of annealing in the Sn0.7Cu+TiO_2 and Sn0.7Cu0.05Ni+TiO_2 samples respectively. A relatively flat and coarse interfacial Cu_6Sn_5 layer and generally larger primary Cu_6Sn_5 particles were observed in reinforced Sn0.7Cu solder joints.

Investigations of the interfacial intermetallic compound layer growth after annealing were carried out by measuring the average thickness of the total interfacial layer (Cu_6Sn_5/$(Cu,Ni)_6Sn_5$ + Cu_3Sn) and Cu_3Sn layer after reflow and annealing. Figure 5a is the average thickness of total interfacial intermetallic compound layer of Sn0.7Cu, Sn0.7Cu+TiO_2, Sn0.7Cu0.05Ni and Sn0.7Cu0.05Ni+TiO_2 solder joints after annealing. Generally, with the increase of annealing time, the total interfacial layer becomes thicker. From the graph, comparing Sn0.7Cu and Sn0.7Cu0.05Ni solder joints, a slightly thinner total interfacial layer of Ni-containing solder joints was observed on as-reflowed samples however it grew thicker than Sn0.7Cu after 500, 1000 and 1500 hours of annealing. After 2000 hours of annealing, the total thickness of the interfacial layer had increased significantly in Sn0.7Cu which resulted in the thickest interfacial layer (~12-13 µm) compared to other solder joints. Across all samples, it was shown that additions of TiO_2 in both Sn0.7Cu and Sn0.7Cu0.05Ni had suppressed the interfacial layer by around 10-40% (compared to no TiO_2) where the suppression percentage increases with the increase in annealing time. Sn0.7Cu0.05Ni+TiO_2 resulted in the thinnest total interfacial layer after 2000 hours of annealing with approximately 6.6 µm total interfacial layer thickness compared to approximately 8.5 µm in Sn0.7Cu0.05Ni.

During early stages of Sn0.7Cu solder wetting, Mohd Salleh et al. (2015b) found that interfacial Cu_6Sn_5 will rapidly form followed by subsequent scallop shaped growth while the Cu_3Sn layer may form in between the Cu_6Sn_5 layer and the Cu as result of continuous Cu diffusion from the substrate into the Cu_6Sn_5 layer. It is reported by Wang et al. (2014) that Cu_3Sn formation could be accelerated by annealing. From Figure 5b, it is observed that in Sn0.7Cu and Sn0.7Cu+TiO2, a significant layer of Cu_3Sn forms changing from ~0.8 µm as-reflowed to ~5 µm after 2000 hours of annealing. However, with Ni additions, a relatively fine and thinner interfacial Cu_3Sn layer were observed indicating the Ni additions were able to suppress the Cu diffusion from the substrate into the Cu_6Sn5 layer. Comparing samples with TiO_2 additions in both Sn0.7Cu and Sn0.7Cu0.05Ni, there is no significant growth or suppression of Cu_3Sn and it appears that TiO_2 does not play a role in controlling the Cu diffusion from the substrate into the layer. It is believed that TiO_2 plays a significant role during the liquid solder wetting where TiO_2 nanoparticles between the liquid solder and substrate acts as a dissolution barrier which reduces the Cu dissolution from the substrate. Thus, excessive reinforcement may also result in a barrier for wetting. After the rapid formation of the Cu_6Sn_5 layer during wetting, TiO_2 nanoparticles may be pushed above the Cu_6Sn_5 layer and remain as a diffusion barrier from the matrix.

Although the TiO_2 nanoparticles density (4.2g/cm^3) is much lower than the liquid Sn (6.98 g/cm^3), a higher surface energy of TiO_2 nanoparticle (~1.9 J/m^2) compared to Sn liquid (~0.5 J/m^2) at 227 ˚C allows the liquid Sn to wet the nanoparticles. During soldering, with 1wt% of TiO_2 additions, some reinforcement will remain in the solder while some particles near the surface were observed to be pushed out during solidification. Stefanescu et al. (1988) reported that when a moving solidification front intercepts an insoluble particle, it can either be pushed or engulfed. Engulfment during solidification occurs when solid grows over the particle, followed by enclosure of the particle in the solid. Evidence of TiO_2 reinforcement remaining on the interfacial Cu_6Sn_5 was observed in deep-etched reinforced solder balls with aggregation of TiO_2 particles as in Figure 4b, 4e (red arrow) and 6. Figure 6a and 6b indicate that TiO_2 may be pushed or engulfed by the interfacial compounds and Sn during solidification. As in Figure 6c, a cup shape of Cu_6Sn_5 can be observed partially surrounding the TiO_2 aggregated particles while being pushed. Figure 6b and 6d confirms the presence of TiO_2 reinforcement by EDS point analysis. Thus, it is possible to use TiO_2 nanoparticles as reinforcement additions in soldering and suppress the total interfacial layer during soldering and annealing. Subsequently by controlling the microstructure in the solder joint, the solder joint strength could be improved.

3.2 Shear strength and fracture energy of solder joints

Mechanical performance of solder joints was conducted by evaluating the shear strength, total shear fracture energy, shear fracture initiation energy and shear fracture propagation energy. Figure 7a represents an example of a high speed solder ball shear strength result comparing as reflowed Sn0.7Cu, Sn0.7Cu+TiO_2, Sn0.7Cu0.05Ni and Sn0.7Cu0.05Ni+TiO_2. As in Figure 7a, the shear force graph of as reflowed Sn0.7Cu and Sn0.7Cu+TiO_2 had a similar trend indicating a more brittle fracture characteristic with a steeper slop before and after the maximum shear force compared to as-reflowed Sn0.7Cu0.05Ni and Sn0.7Cu0.05Ni+TiO_2 which indicates a more ductile fracture solder joint. Tsukamoto et al. (2010) reported that from a shear force graph, a steeper slope indicates a more brittle fracture characteristic. Results of the shear strength of each solder joint composition after annealing are plotted in Figure 7b. With 1wt%TiO_2 in the as-reflowed samples, the solder joint strength of Sn0.7Cu had increased by about 20% of the average shear strength while the addition of 0.05wt%Ni had increased by

about 28% (~16 N) of the average shear strength. The Sn0.7Cu0.05Ni+TiO_2 samples had the highest average solder joint strength among all the solder joints of approximately 16.5 N while Sn0.7Cu resulted in the lowest average solder joint strength of approximately 12.5 N. Annealed solder joints had a relatively decreasing values of average shear strength after 500, 1000, 1500 and 2000 hours of annealing time. At the maximum annealing time (2000 hour), it was observed that solder joints with the additions of TiO_2 had the highest average shear strength with a similar strength between Sn0.7CuTiO_2 and Sn0.7Cu0.05Ni+TiO_2. This indicates that TiO_2 additions had improved the solder joint strength in all annealed samples and a combination of 0.05wt%Ni and TiO_2 to Sn0.7Cu resulted in the highest shear strength. Referring to the total interfacial intermetallic thickness and the Cu_3Sn interfacial thickness (Figure 4a and b) after annealing, the shear strength of the solder joint decreases as the thickness of these interfacial layer increases. It is believed that besides the suppression of the interfacial layer, TiO_2 could also act to pin dislocations in the solder joint matrix which increases the solder joint. However, it is known that solder joint strength does not only rely on the interfacial layer thickness and could also be influenced by other factors such as flux void formation, Kirkendall void formation and large primary intermetallics in the solder joint matrix.

Figure 8 shows the total shear energy, fracture initiation energy and fracture propagation energy of the solder joint samples at 0, 500, 1000, 1500 and 2000 hours of annealing. Sn0.7Cu0.05Ni+TiO_2 resulted in the highest shear energy value compared to other solder joint compositions. In contrast, Sn0.7Cu had the lowest shear energy value. It is observed that with an increasing annealing time, the total shear energy of Sn0.7Cu0.05Ni and Sn0.7Cu0.05Ni+TiO_2 decreased while Sn0.7Cu and Sn0.7Cu+TiO2 did not display a decreasing shear energy value after annealing. This may be due to the low shear energy in as-reflowed samples of Sn0.7Cu and Sn0.7Cu+TiO_2 which indicates a brittle fracture threshold value even before annealing. By distinguishing the fracture initiation and propagation energy, the relative energy required for a solder joint fracture to initiate and propagate could be determined. As shown in Figure 8b, fracture initiation energy of solder joints had a similar trend to the total fracture initiation energy. On as-reflowed solder joints, for Sn0.7Cu0.05Ni+TiO2, approximately 1.8 mJ is required to initiate a solder joint fracture and this decreases after annealing time to 2000 hours to approximately 0.9 mJ. Similarly a decreasing trend of Sn0.7Cu0.05Ni fracture initiation energy is apparent, where the approximately 1.6 mJ is required to initiate a solder joint fracture decreases after annealing for

2000 hours to approximately 0.8 mJ. The fracture propagation energy of the sheared solder joints is shown in Figure 8c and it is seen in as-reflowed solder joints and after 2000 hours of annealing, Sn0.7Cu0.05Ni+TiO2 resulted in the highest value compared to other solder joints. However, no obvious trend in fracture propagation energy in all solder joints after annealing was apparent.

3.3 Fracture surface analysis

Figure 9 and Figure 10 show the fracture mode distributions of the high speed shear solder joint samples collected from SEM images based on the failure modes defined in Figure 1c-f. Figure 9a indicates the fracture mode distribution of Sn0.7Cu in as-reflowed solder joints and annealed solder joints. It is observed that the majority of the fracture modes for this solder joint composition were relatively brittle and a small percentage of quasi-brittle failure was observed. When TiO_2 additions were made to Sn0.7Cu, a less brittle fracture was observed and quasi-brittle failure dominated. It is likely the suppression of the total interfacial layer thickness as in Figure 4a has influenced the fracture mode and a reduced interfacial layer thickness resulted in more fracture in the bulk solder which resulted in quasi-brittle and quasi ductile failure modes at 2000 hours in annealed solder joints. In Sn0.7Cu0.05Ni and with the additions of TiO_2, less brittle failure was observed. After annealing to 2000 hours, 100% of samples experienced quasi-brittle failure in Sn0.7Cu0.05Ni solder joints while with TiO_2 additions, a mixture of ductile, quasi-ductile and quasi-brittle failure modes were observed. It is apparent therefore that Ni and TiO_2 additions can alter the failure mode from a more brittle failure mode to a more ductile failure mode. This may be attributed to a suppression of the Cu_3Sn layer and the total interfacial layer thickness. Koo et al. (2008) found that the Cu_3Sn layer may also be associated with Kirkendall voids which become more prevalent in annealed solder joints.

For a clearer understanding on the factors that affect the failure modes, fracture surfaces were analysed. Figure 11 and 12 shows the SEM image of the fracture surfaces of all sheared solder joints after 2000 hours of annealing. As in Figure 11a and b in the Sn0.7Cu fracture surface, failure modes of brittle and quasi-brittle were majorly caused by the formation of Kirkendall voids with the sheared solder joint fracturing predominantly through the Cu_3Sn and Cu_6Sn_5 layer. From the fracture surface of the Cu_3Sn layer as in Figure 11b, the Kirkendall voids played a major role. With additions of TiO_2, although a thick layer of Cu_3Sn was measured in the

solder joints, the majority of the fracture surface was through the large Cu_6Sn_5 interfacial layer and the bulk solder. In both samples, intergranular brittle cracks were observed (indicated by red arrows) on the Cu_6Sn_5 interfacial scallop grooves where large Cu_6Sn_5 scallop grooves were observed in cross section image of the interfacial layer as in Figure 2d and h.

Figure 12a and b are detailed fracture surfaces of Sn0.7Cu0.05Ni sheared solder joints after 2000 hours of annealing which show quasi-brittle failure modes of the solder joints were through the $(Cu,Ni)_6Sn_5$ layer and bulk solder. Evidence of the existence of solder voids were observed where cup-shaped fracture was observed in the bulk solder as indicated with the red arrow in Figure 12b. Fracture surfaces of Sn0.7Cu0.05Ni+TiO_2 as in Figure 12c and d show fracture of the solder joints occured through the bulk solder, Cu_3Sn and $(Cu,Ni)_6Sn_5$ layer. At the bulk solder near to the surface of the solder ball, primary $(Cu,Ni)_6Sn_5$ cracks were observed. These brittle primary intermetallics which exists at the edge of the solder ball may act as a weak point where fracture may initiate.

4.0 Conclusions

The effects of Ni, TiO_2 in isolation and when combined on the microstructure and properties of Sn0.7Cu solders on Cu substrates were examined for a range of annealing times.

The following conclusion can be made:

a) A scallop-shaped interfacial Cu_6Sn_5 layer with a planar layer of Cu_3Sn formed when using Sn0.7Cu. With additions of TiO_2 reinforcement to Sn0.7Cu, a more planar scalloped Cu_6Sn_5 morphology was present with reduced interfacial boundary grooves. A fine scallop-shaped interfacial $(Cu,Ni)_6Sn_5$ layer was present when using Sn0.7Cu0.05Ni and Sn0.7Cu0.05Ni+TiO_2.
b) Additions of TiO_2 to both Sn0.7Cu and Sn0.7Cu0.05Ni suppressed the total interfacial layer by 10-40% with the suppression percentage increasing with an increase in annealing time.
c) Kirkendall voids on the Cu_3Sn layer were observed to increase after longer annealing times where a fine and significantly thinner interfacial Cu_3Sn layer was observed in solder joints containing Ni. This shows that Ni was able to suppress the Cu diffusion from the substrate into the Cu_6Sn5 layer and suppress the Cu_3Sn layer.

d) Evidence of TiO_2 reinforcement remaining on the interfacial Cu_6Sn_5 in deep etched reinforced solder balls indicates that TiO_2 may be pushed or engulfed by the interfacial layer growth and Sn during solidification. TiO_2 nanoparticles between the liquid solder and substrate may act as a dissolution barrier which reduces the Cu dissolution from the substrate during soldering and remain as a diffusion barrier from the matrix during annealing.

e) The solder joint strength of solders containing TiO_2 increased by about 20%-28% of the average shear strength compared to non-reinforced solder joints and Sn0.7Cu0.05Ni+TiO2 displayed the highest average solder joint shear strength and total fracture energy among all the solder joints after reflow and subsequent annealing.

f) Ni and TiO_2 additions altered the failure mode from brittle to a more ductile failure mode. This was attributed to the suppression of the Cu_3Sn layer and the total interfacial layer thickness.

5.0 Acknowledgement

This work was financially supported from the University of Queensland (UQ)-Nihon Superior (NS) collaboration research project, ARC Linkage project (LP140100485) and scholarship from the Malaysian Higher Education Ministry and University Malaysia Perlis (UniMAP). Authors would like to thank Mr. Xuan Quy Tran for his kind help in preparing the metallography samples. High speed shear tests were conducted at Nihon Superior Japan.

References

Chellvarajoo, S., Abdullah, M.Z., 2016. Microstructure and mechanical properties of Pb-free Sn–3.0Ag–0.5Cu solder pastes added with NiO nanoparticles after reflow soldering process. Materials & Design 90, 499-507.

Chuang, C.-M., Lin, K.-L., 2003. Effect of microelements addition on the interfacial reaction between Sn-Ag-Cu solders and the Cu substrate. Journal of Electronic Materials 32, 1426-1431.

Chuang, T.H., Wu, M.W., Chang, S.Y., Ping, S.F., Tsao, L.C., 2010. Strengthening mechanism of nano-Al2O3 particles reinforced Sn3.5Ag0.5Cu lead-free solder. Journal of Materials Science: Materials in Electronics 22, 1021-1027.

El-Daly, A.A., Fawzy, A., Mansour, S.F., Younis, M.J., 2013. Novel SiC nanoparticles-containing Sn–1.0Ag–0.5Cu solder with good drop impact performance. Materials Science and Engineering: A 578, 62-71.

Koo, J.-M., Kim, Y.-N., Yoon, J.-W., Kim, D.-G., Noh, B.-I., Kim, J.-W., Moon, J.-H., Jung, S.-B., 2008. Effect of displacement rate on bump shear properties of electroplated solder bumps in flip-chip packages. Materials Science and Engineering: A 483–484, 620-624.

Liu, X.D., Han, Y.D., Jing, H.Y., Wei, J., Xu, L.Y., 2013. Effect of graphene nanosheets reinforcement on the performance of Sn-Ag-Cu lead-free solder. Materials Science and Engineering: A 562, 25-32.

Mohd Salleh, M.A.A., Bakri, A.M.M.A., Kamarudin, H., Bnhussain, M., M.H, Z.H., Somidin, F., 2011. Solderability of Sn-0.7Cu/Si3N4 lead-free composite solder on Cu-substrate. Physics Procedia 22, 299-304.

Mohd Salleh, M.A.A., Bakri, A.M.M.A., Zan@Hazizi, M.H., Somidin, F., Mohd Alui, N.F., Ahmad, Z.A., 2012. Mechanical properties of Sn–0.7Cu/Si3N4 lead-free composite solder. Materials Science and Engineering: A 556, 633-637.

Mohd Salleh, M.A.A., McDonald, S.D., Gourlay, C.M., Belyakov, S.A., Yasuda, H., Nogita, K., 2016a. Effect of Ni on the Formation and Growth of Primary Cu6Sn5 Intermetallics in Sn-0.7 wt.%Cu Solder Pastes on Cu Substrates During the Soldering Process. Journal of Electronic Materials 45, 154-163.

Mohd Salleh, M.A.A., McDonald, S.D., Gourlay, C.M., Yasuda, H., Nogita, K., 2016b. Suppression of Cu6Sn5 in TiO2 reinforced solder joints after multiple reflow cycles. Materials & Design 108, 418-428.

Mohd Salleh, M.A.A., McDonald, S.D., Terada, Y., Yasuda, H., Nogita, K., 2015a. Development of a microwave sintered TiO2 reinforced Sn–0.7wt%Cu–0.05wt%Ni alloy. Materials & Design 82, 136-147.

Mohd Salleh, M.A.A., McDonald, S.D., Yasuda, H., Sugiyama, A., Nogita, K., 2015b. Rapid Cu6Sn5 growth at liquid Sn/solid Cu interfaces. Scripta Materialia 100, 17-20.

Mohd Salleh, M.M.A., McDonald, S., Nogita, K., 2013. Non-metal reinforced lead-free composite solder fabrication methods and its reinforcing effects to the suppression of intermetallic formation: Short review, Applied Mechanics and Materials, pp. 260-266.

Said, R.M., Salleh, M.A.A.M., Derman, M.N., Ramli, M.I.I., Nasir, N.M., Saud, N., 2016. Isothermal aging affect to the growth of Sn-Cu-Ni-1 wt. % TiO<inf>2</inf> composite solder paste, Key Engineering Materials, pp. 123-131.

Shen, J., Chan, Y.C., 2009. Effects of ZrO2 nanoparticles on the mechanical properties of Sn–Zn solder joints on Au/Ni/Cu pads. Journal of Alloys and Compounds 477, 552-559.

Shohji, I., Tsunoda, S., Watanabe, H., Asai, T., Nagano, M., 2005. Reliability of solder joint with Sn-Ag-Cu-Ni-Ge lead-free alloy under heat exposure conditions. Materials Transactions 46, 2737-2744.

Somidin, F., Salleh, M.A.A., Ahmad, K.R., 2013. Intermetallic compound formation on solder alloy/cu-substrate interface using lead-free Sn-0.7Cu/recycled-aluminum composite solder, Advanced Materials Research, pp. 105-111.

Stefanescu, D.M., Dhindaw, B.K., Kacar, S.A., Moitra, A., 1988. Behavior of ceramic particles at the solid- liquid metal interface in metal matrix composites. Metallurgical Transactions A 19, 2847-2855.

Tsao, L.C., Huang, C.H., Chung, C.H., Chen, R.S., 2012. Influence of TiO2 nanoparticles addition on the microstructural and mechanical properties of Sn0.7Cu nano-composite solder. Materials Science and Engineering: A 545, 194-200.

Tsukamoto, H., Nishimura, T., Suenaga, S., Nogita, K., 2010. Shear and tensile impact strength of lead-free solder ball grid arrays placed on Ni (P)/Au surface-finished substrates. Materials Science and Engineering: B 171, 162-171.

Wang, K.-K., Gan, D., Hsieh, K.-C., 2014. The orientation relationships of the Cu3Sn/Cu interfaces and a discussion of the formation sequence of Cu3Sn and Cu6Sn5. Thin Solid Films 562, 398-404.

Yu, C., Chen, J., Cheng, Z., Huang, Y., Chen, J., Xu, J., Lu, H., 2016. Fine grained Cu film promoting Kirkendall voiding at Cu3Sn/Cu interface. Journal of Alloys and Compounds 660, 80-84.

Zeng, G., McDonald, S.D., Mu, D., Terada, Y., Yasuda, H., Gu, Q., Nogita, K., 2014. Ni segregation in the interfacial (Cu,Ni)6Sn5 intermetallic layer of Sn-0.7Cu-0.05Ni/Cu ball grid array (BGA) joints. Intermetallics 54, 20-27.

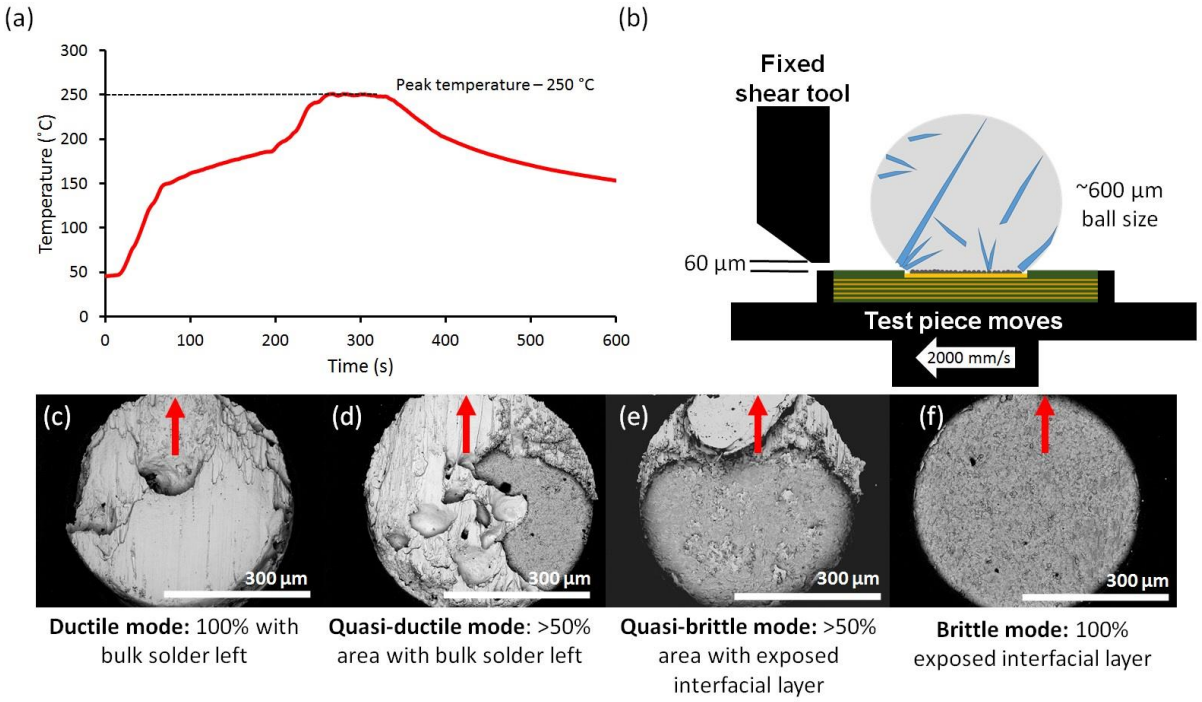

Figure 1: a) Solder reflow temperature profile for solder joint fabrication, b) high speed shear test setup and sample positioning and (c-f) backscattered electron SEM images of four different main solder joint fracture modes after high speed shear testing.

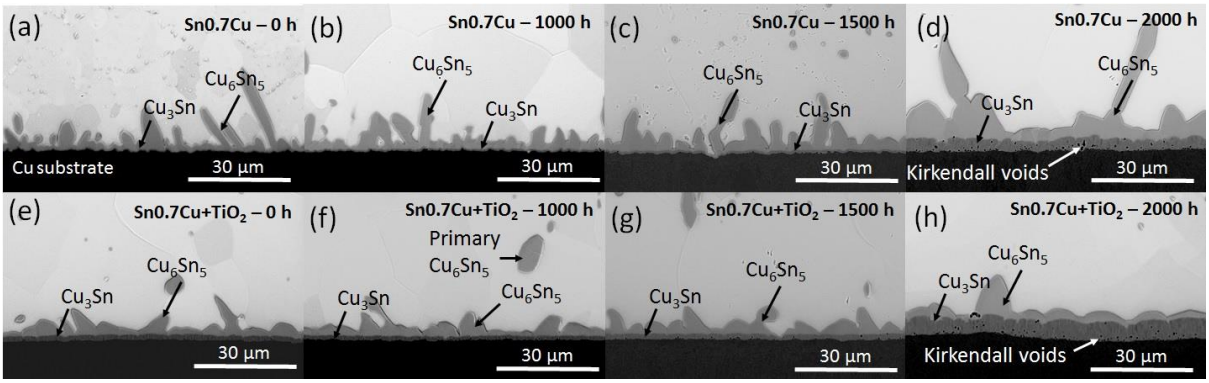

Figure 2: Backscattered electron SEM images of the interfacial Cu_6Sn_5 and Cu_3Sn intermetallic compound layers in annealed Sn0.7Cu after (a) 0 hours, (b) 1000 hours, (c) 1500 hours, (d) 2000 hours and Sn0.7Cu+TiO_2 after (e) 0 hours, (f) 1000 hours, (g) 1500 hours, (h) 2000 hours.

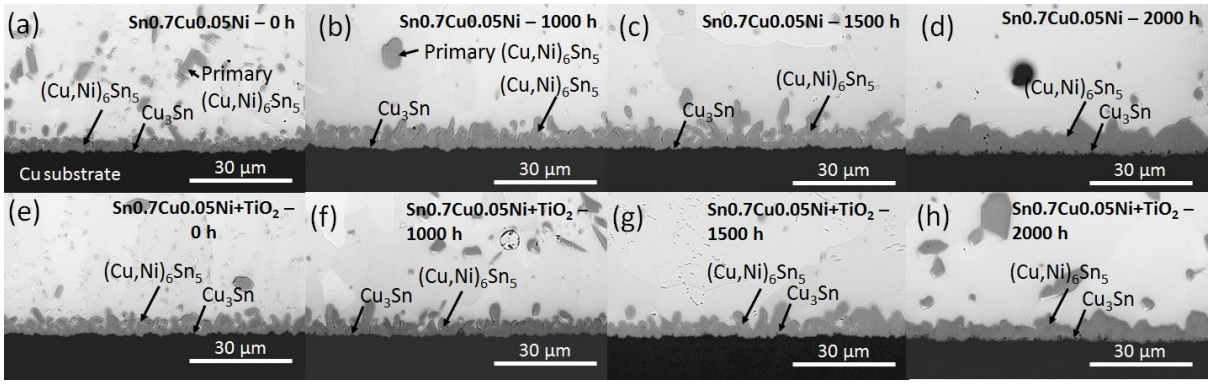

Figure 3: Backscattered electron SEM images of interfacial $(Cu,Ni)_6Sn_5$ and the Cu_3Sn intermetallic compound layers in annealed Sn0.7Cu0.05Ni after (a) 0 hours, (b) 1000 hours, (c) 1500 hours, (d) 2000 hours and Sn0.7Cu0.05Ni+TiO_2 after (e) 0 hours, (f) 1000 hours, (g) 1500 hours, (h) 2000 hours.

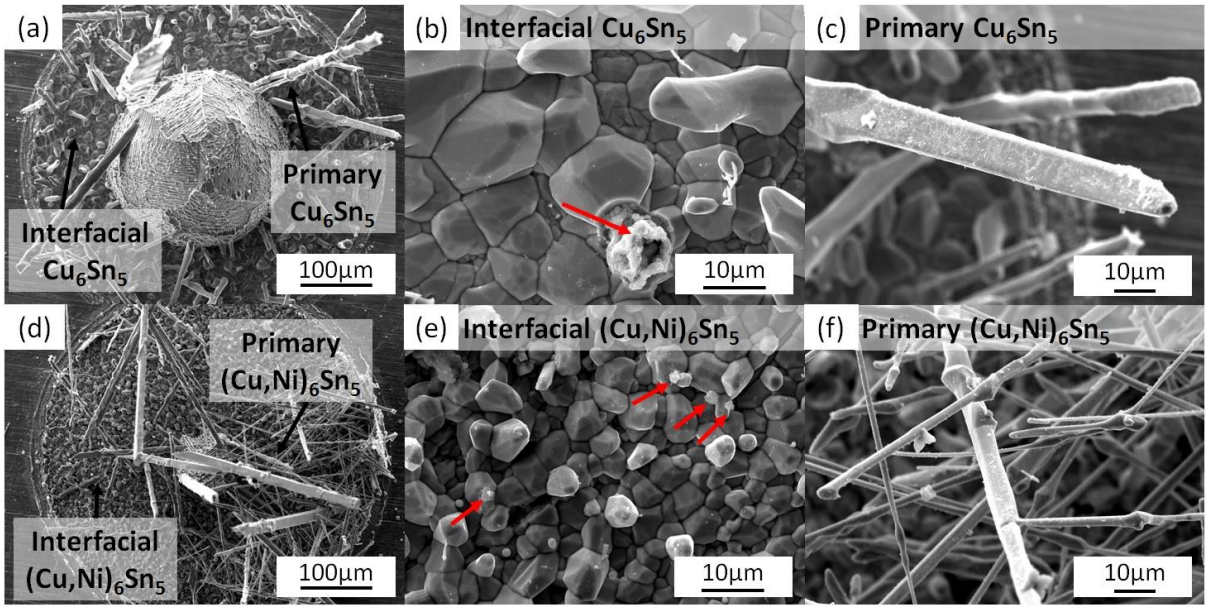

Figure 4: Secondary electron SEM images of deep etched solder joints after 2000 hours of isothermal annealing revealing the primary and interfacial intermetallic compounds of (a-c) Sn0.7Cu+TiO_2 and (d-f) Sn0.7Cu0.05Ni+TiO_2.

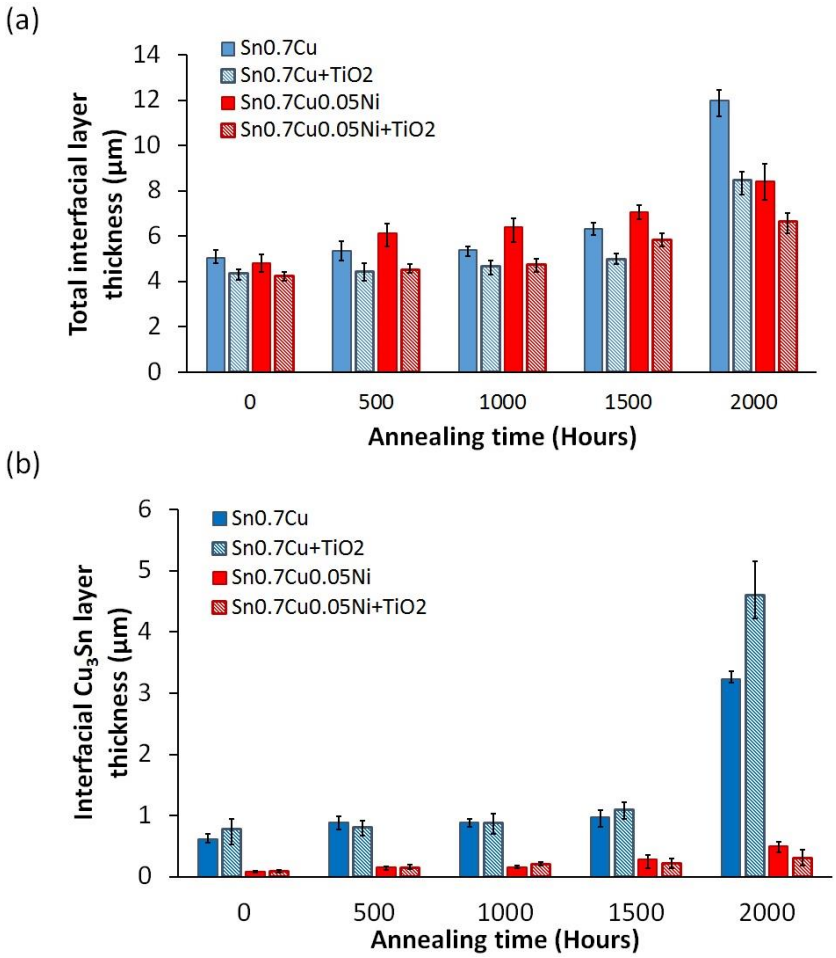

Figure 5: Average thickness of the (a) total interfacial intermetallic compound, (b) interfacial $Cu_6Sn_5/(Cu,Ni)_6Sn_5$ intermetallic compound and (c) interfacial Cu_3Sn layer formation of isothermal annealed Sn0.7Cu, Sn0.7Cu+TiO_2, Sn0.7Cu0.05Ni and Sn0.7Cu0.05Ni+TiO_2 after 0, 500, 1000, 1500 and 2000 hours.

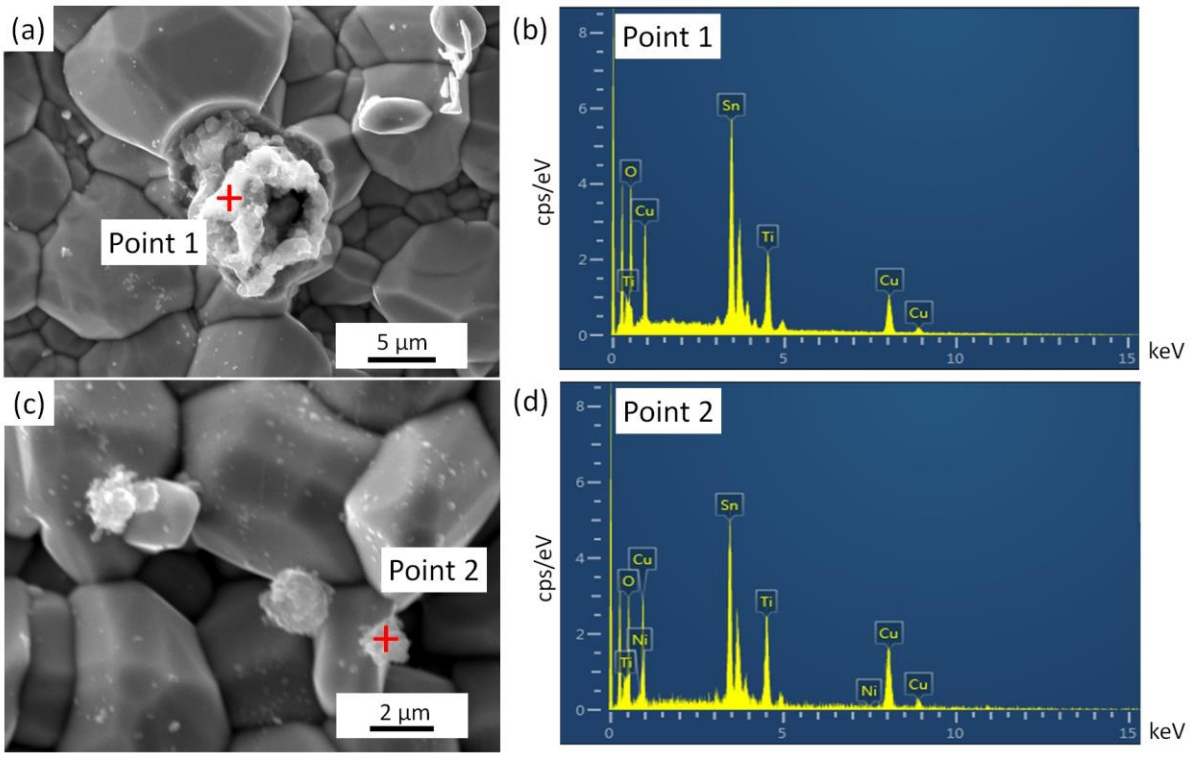

Figure 6: Secondary electron SEM images and EDS point analysis of agglomerated TiO_2 found attached to the interfacial layers of (a-b) Sn0.7Cu+TiO_2 and (c-d) Sn0.7Cu0.05Ni+TiO_2 after 2000 hour isothermal annealing.

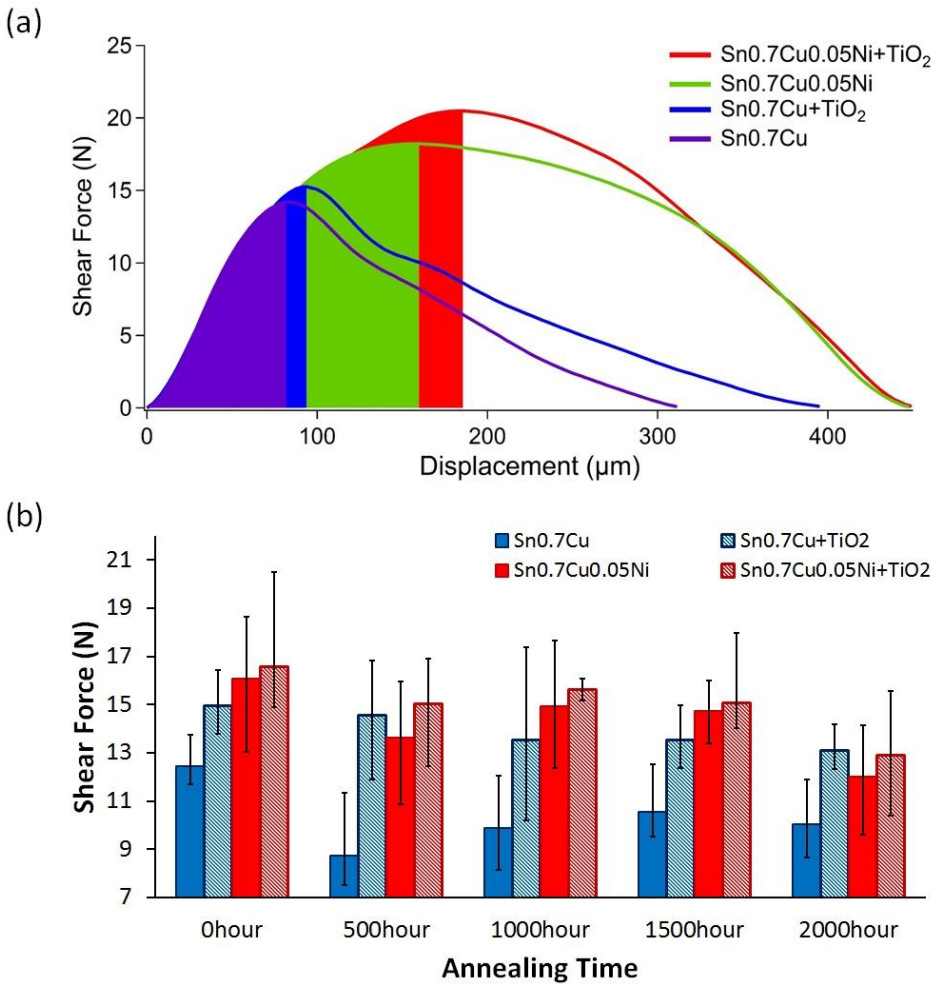

Figure 7: (a) Shear force versus displacement graph for high speed shear tests with the colored area showing the initial fracture energy of the as-soldered solder joint samples and (b) the shear force indicating the shear strength of solder joints after 0, 500, 1000, 1500 and 2000 hours of isothermal annealing.

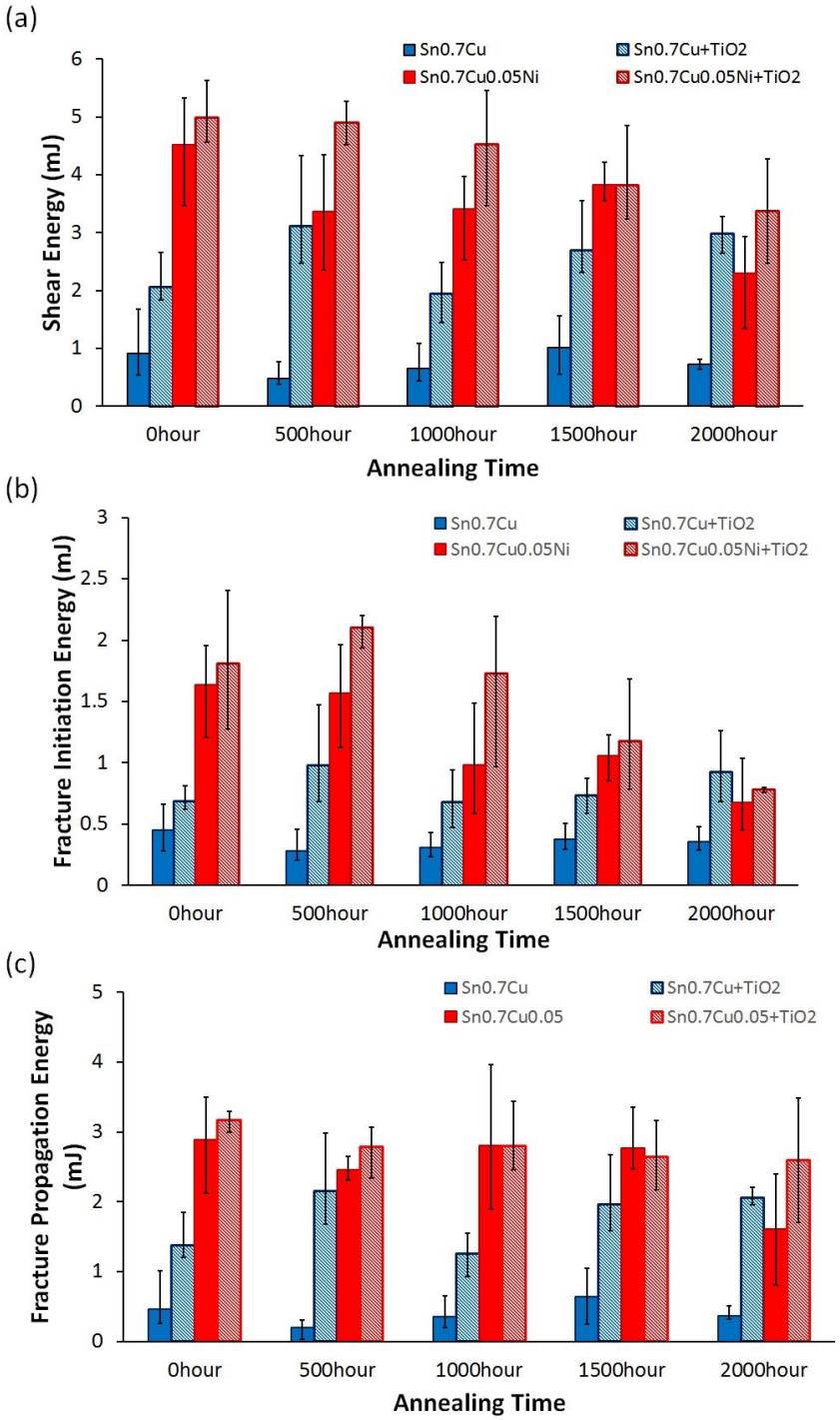

Figure 8: (a) Total shear energy, (b) fracture initiation energy and (c) fracture propagation energy of 0, 500, 1000, 1500 and 2000 hour isothermal annealed solder joints.

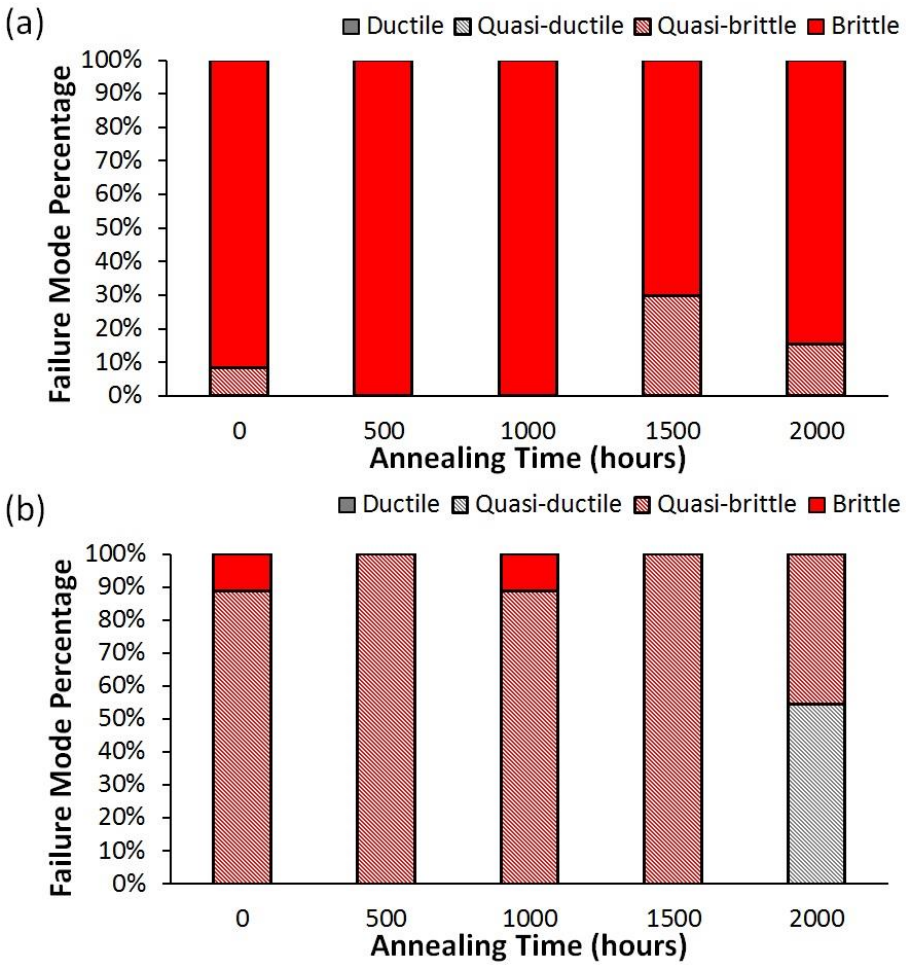

Figure 9: Fracture mode distribution of high speed shear results of annealed solder joints of (a) Sn0.7Cu and (b) Sn0.7Cu+TiO_2 after 0, 500, 1000, 1500 and 2000 hours.

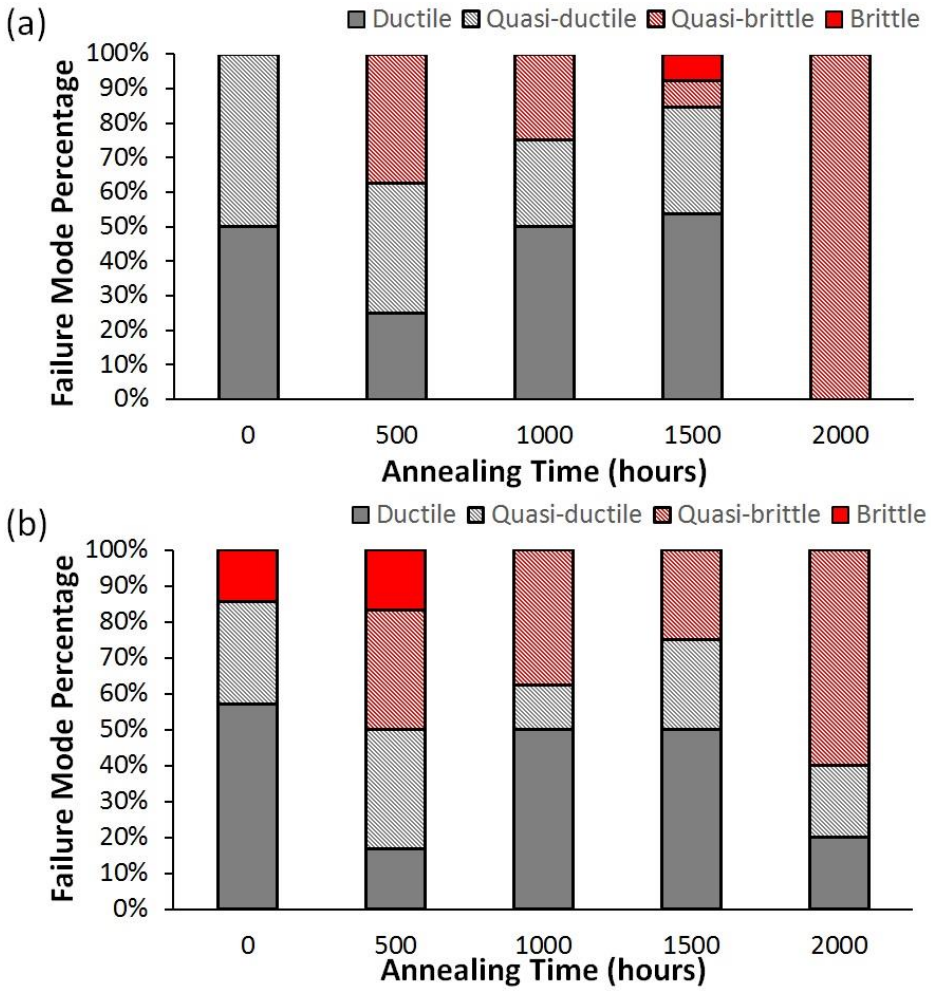

Figure 10: Fracture mode distribution of high speed shear results of annealed solder joints of (a) Sn0.7Cu0.05Ni and (b) Sn0.7Cu0.05Ni+TiO_2 after 0, 500, 1000, 1500 and 2000 hours.

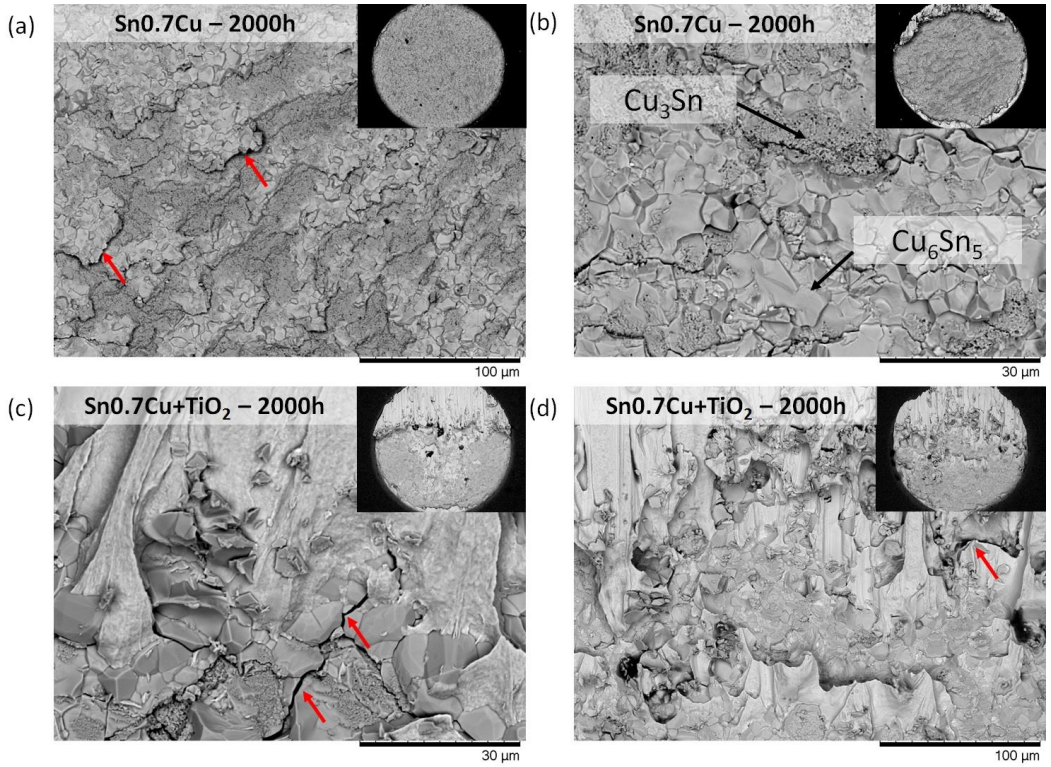

Figure 11: Detailed surface fracture backscattered electron SEM images of (a) brittle mode Sn0.7Cu annealed for 2000 hours, (b) quasi brittle mode Sn0.7Cu annealed for 2000 hours, (c) quasi brittle mode Sn0.7Cu+TiO_2 annealed for 2000 hour and (d) quasi ductile mode Sn0.7Cu annealed for 2000 hours. Red arrows indicate the intergranular brittle cracks at the Cu_6Sn_5 grooves.

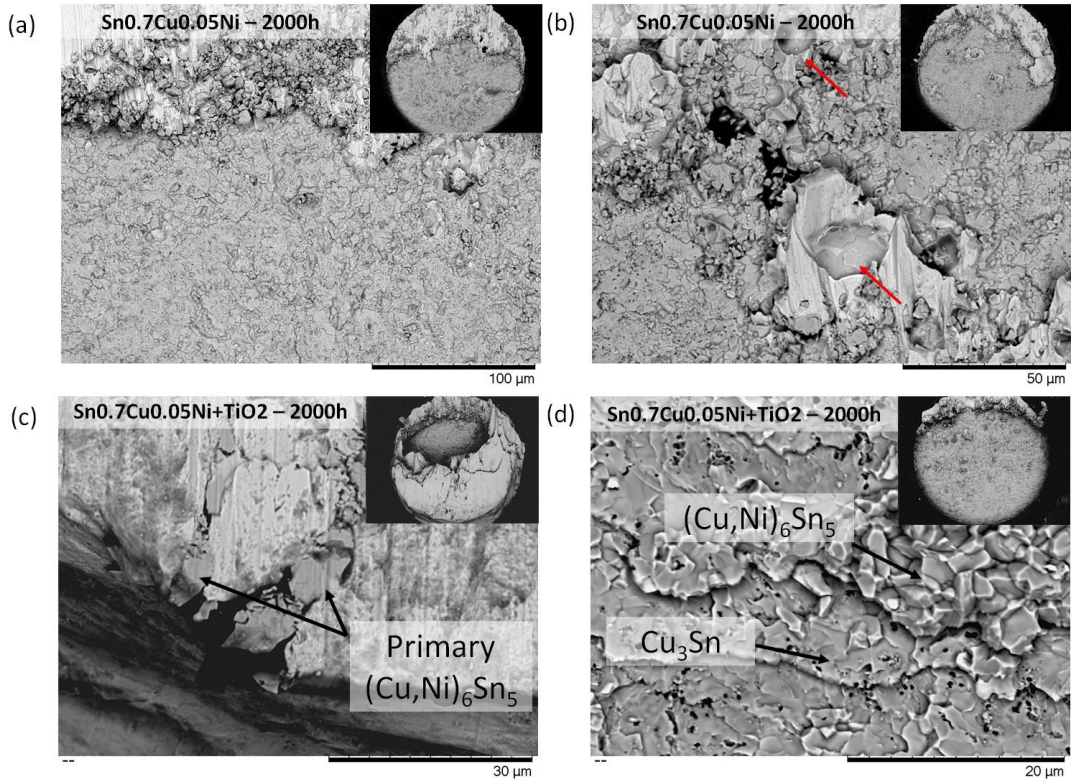

Figure 12: Detailed surface fracture backscattered electron SEM images of (a-b) quasi brittle mode Sn0.7Cu0.05Ni annealed for 2000 hours, (c) quasi ductile mode Sn0.7Cu0.05Ni+TiO_2 annealed for 2000 hours and (d) quasi brittle mode Sn0.7Cu0.05Ni+TiO_2 annealed for 2000 hours. Red arrows in (b) indicate the interfacial solder voids at the fracture surface.

Table 1: Chemical composition of the Sn0.7Cu powder.

	Sn	Cu	Ag	Fe	Bi	Al	Cd	Ni	Sb	Zn	Pb	As	Hg
Composition (wt%)	Balance	0.686	0.009	0.006	0.013	<0.001	<0.001	<0.002	0.020	<0.001	0.008	<0.005	<0.001

Table 2: Chemical composition of the Sn0.7Cu0.05Ni powder.

	Sn	Cu	Ni	Sb	Bi	Zn	Al	As	Sb	Cd	Pb
Composition (wt%)	Balance	0.620	0.056	0.08	0.013	<0.001	<0.001	<0.002	0.020	<0.001	0.686